Leading-Edge Slat Design by a Semi-Inverse Technique

JOHN E. O'PRAY*
United States Air Force Rocket Propulsion Laboratory, Edwards Air Force Base, Calif.
AND
PETER B. S. LISSAMAN†
Northrop Corporate Laboratories, Hawthorne, Calif.

A method of generating high-lift leading-edge slats for arbitrary airfoils is developed. The technique assumes that a desirable pressure distribution for the main airfoil is specified from boundary-layer considerations. Using conformal transformations, slats which generate pressure distributions having a least squares matching to the specified distribution are developed. The approximate slat chord, position, and thickness are selected, and the semi-inverse solution then generates the slat camber distribution required to achieve the desired modulation. Accurate matchings to the specified pressure distributions are achieved for the elliptical airfoil test cases. Predicted pressure distributions on the airfoil and on the slat generated by the semi-inverse solution compare well with pressures computed by a direct numerical solution. Small, thin, highly cambered slats located close to the airfoil nose are found to be desirable. As a design tool, the method rapidly develops a family of slats which will induce the desired modulation on the airfoil.

Introduction

IT has long been known that leading-edge slats could improve the performance of airfoils by suppressing or delaying nose stall through the modulation of pressure gradients at the leading edge of the main airfoil. The first patent on the leading-edge slat was applied for by G. V. Lachmann in 1918, and later this device was extensively developed by Lachmann and Handley-Page.[1]

At high values of circulation, an airfoil of moderate camber experiences a strong flow around the leading edge. This flowfield depends principally on the circulation and the nose radius. The circulation is induced by the Kutta conditions at the trailing edge, and many different flap arrangements will create the same gross nose flow. The details of the flowfield at the nose, however, depend almost entirely on the nose radius, with the circulation providing principally a scaling factor.

For thin airfoils with small nose radii, there is a severe suction peak at the nose followed by highly adverse pressure gradients which may induce boundary-layer separation. The addition of a slat with its associated vorticity superimposes a backflow component in the nose region which, by reducing velocities on the main airfoil and moderating the pressure gradients, prevents separation as is schematically illustrated in Fig. 1. The boundary layer on the airfoil can be assumed to be thin with respect to the slat gap due to the extremely favorable pressure gradients it experiences from the stagnation point forward to the minimum pressure point.[2] Thus the fluid mechanics of the slat may be treated as a potential flow with only minor displacement effects from the thin, attached boundary layer. In fact, it appears that if the slat and main airfoil boundary layers do interact near the airfoil nose, then it is a poor slat design.

In 1922, Lachmann, on the suggestion of Prandtl and Betz, developed a restricted analytical theory for slat performance using a conformal mapping for the airfoil with the slat represented as a vortex singularity distribution.[2] Today, standard methods are available for the direct problem which is the determination of the flowfield for a given slat and airfoil geometry. These methods cannot be used, however, to generate a required flowfield on an arbitrary main airfoil except by trial and error.

The objective of the semi-inverse solution presented here is to provide a technique which will enable a designer, given a main airfoil of fixed geometry and angle of attack, to generate a family of slats which can create the desired pressure modulation on the nose of the main airfoil. The desired pressure distribution on the airfoil nose is one which has adverse pressure gradients which are sufficiently mild to avoid separation. This method is not intended to give an exact inverse solution. Instead, this technique will generate a class of slats, all of which have induced velocity fields which closely approximate the modulation required. From this class of slats, the particular configuration which is most attractive in terms of structure, retracted profile, or other considerations can be selected. A direct numerical solution for multi-element airfoils which includes viscous effects can then be used to determine the exact pressure distributions and to verify that the boundary layers on the slat and airfoil will remain attached. This method had been developed as a design tool, and has the flexibility to accommodate various constraints. For example, the slat nose radius and thickness distribution may be prescribed. The program will then generate a slat conforming to these constraints.

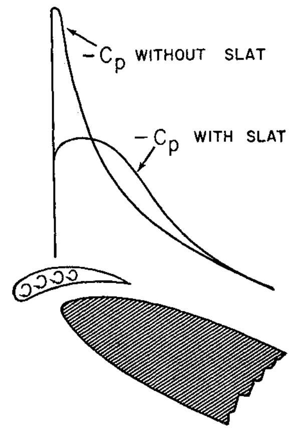

Fig. 1 Modulation of airfoil nose pressure distribution by leading-edge slat.

Presented as Paper 71-11 at the AIAA 9th Aerospace Sciences Meeting, New York, January 25–27, 1971; submitted January 25, 1971; revision received September 16, 1971.

* 1st Lt. USAF. Project Engineer. Associate Member AIAA.

† Director, Continuum Mechanics Laboratory. Member AIAA.

Analysis

As an introduction to the analysis, it is helpful to describe the basic steps leading to the formulation of the potential flow problem. First, the theoretical pressure distribution on the airfoil without a slat is computed. Using a suitable boundary-layer analysis, a desirable, separation-free pressure distribution is determined for approximately the first 10% of the airfoil chord.[3,4] The difference between the unacceptably severe theoretical pressure distribution on the unslatted airfoil and the desired separation-free distribution is designated the specified nose pressure modulation. The analysis which follows describes the process of finding a connected set of off-surface singularities which will induce this specified modulation. The authors stress that this paper is not concerned with either the boundary-layer criteria for defining acceptable pressure distributions or the general airfoil mapping problem.

By mapping the airfoil to a circle using standard techniques, the basic potential flow problem may be formulated as that of determining the singularities required to generate a prescribed flow about a circle. Removing the flow component due to the main stream, we are left with the problem of determining the slat singularities required to induce a specified modulating velocity field on a circle in a still fluid. This now becomes a well-set problem which is amenable to complex theoretic analysis. It is clear that an arbitrary modulation will not necessarily correspond to a connected sheet of singularities. Physically, this implies that there may be no single slat which can induce an arbitrarily prescribed modulation. An analytic continuation of the flowfield on the circle will certainly define a set of off-surface singularities which could create the field. However, these singularities may be nonunique, and there is no assurance that any resultant body is either closed or simply connected. It is clear from elementary considerations that the condition that the total slat source strength be zero is a necessary condition for slat closure. In this semi-inverse solution, connectivity of the slat is assured by prescribing that the slat singularities form a single source-vortex sheet of strength determined by a least squares matching to the desired modulation. A more comprehensive discussion of the existence and uniqueness of the slat singularities is given in Ref. 5.

By standard mappings, the circle is then transformed into an infinite straight line with the slat singularities in the halfplane above it. Thus the problem becomes that of determining the distribution of singularities along the single source-vortex sheet which is necessary to produce the prescribed field on the line. In this half-plane, the geometry is similar for all airfoils, and therefore, the basic semi-inverse solution becomes fully general.

In passing, it should be noted that the common availability of exact, numerical, direct solutions for general airfoils insures that the circle mapping can be readily determined.[6] Any single potential flow solution for the airfoil implicitly provides the mapping because of the point-to-point correspondence between the calculated potential on the airfoil and the known potential on the circle.

Mapping to the Half-Plane

The trial solutions were conducted for an elliptical main airfoil. However, because any airfoil can be mapped into a circle and hence an ellipse, this does not restrict generality. As a matter of fact, for most airfoils without extreme leading edge camber, the nose is very nearly elliptical.[7] Thus the airfoil-to-ellipse mapping is almost one-to-one in the nose region. The complex potential is conserved throughout this geometrical mapping sequence.

The inverse Joukowski transformation is used to map the elliptical airfoil of thickness ratio $T = b/a$ in the Z plane into a circle of radius $c_3 = (a+b)/2$ in the z plane. This circle is then mapped to the upper half-plane $I(W) \geq 0$ (here R and I are used respectively to designate the real and imaginary parts of a complex function). This is achieved by the bilinear transformation

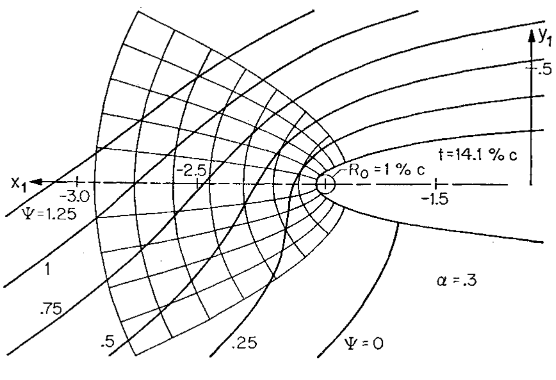

Fig. 2 Ellipse plane nose flow.

$$W = i(z + c_3)/(z - c_3) \qquad W = x_3 + iy_3 \tag{1}$$

This mapping opens the ellipse at the trailing edge, unfolds it about the leading edge to a straight line, and, by a rotation of $\pi/2$, maps the ellipse surface onto the real axis in the W plane with the nose at the origin. The ellipse trailing-edge maps to infinity in the half-plane, and the circle at infinity in the ellipse plane collapses to the point $W = +i$. The nose region for the particular ellipse used as a test case is shown in Fig. 2, and the transformation of this region into the half plane is shown in Fig. 3. Corresponding orthogonal coordinate grids are plotted in each of the domains.

By substituting the inverse of the circle plane to half-plane transformation, Eq. (1), into the well-known equation for the complex potential $F(z)$ of a lifting cylinder in a uniform onset stream, the complex potential $F(W)$ for the main flow in the half-plane can be expressed in the following form

$$F(W) = Uc_3\left[e^{-i\alpha}\left(\frac{W+i}{W-i}\right) + e^{+i\alpha}\left(\frac{W-i}{W+i}\right)\right] + i\left(\frac{\Gamma_t}{2\pi}\right)\log\left(\frac{W+i}{W-i}\right) + \alpha\left(\frac{\Gamma_t}{2\pi}\right) \tag{2}$$

For the lifting, unslatted ellipse at an angle of attack α in a uniform onset flow with velocity U, the total circulation Γ_t required to establish the Kutta condition at the ellipse trailing edge is $\Gamma_t = 4\pi U c_3 \sin\alpha = \Gamma_o$.

The streamline pattern around the nose of the ellipse provides significant insight into the flow in which the leading-edge slat is immersed. For the test case ellipse, the streamlines around the ellipse nose are shown in Fig. 2, and the corresponding flow pattern in the half-plane is shown in Fig. 3. The flow at infinity in the ellipse and circle planes collapses to an inclined vortex doublet at $W = +i$ in the half-plane. A small region above and to the right of the origin

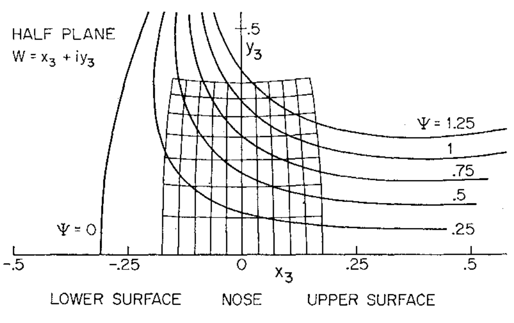

Fig. 3 Main flow in half-plane.

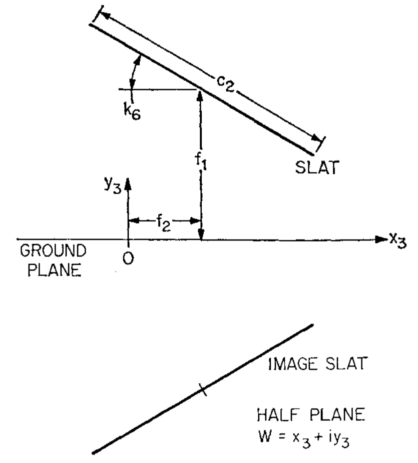

Fig. 4 Slat and image slat geometry.

in the half-plane is the domain for effective slats. In this region, the mild curvature of the main flow streamlines permits representation of the slat chord line as a straight line segment which is locally parallel to a streamline.

An additional transformation from the half-plane to the slat-centered half-plane or slat plane is introduced so that the expressions for the induced velocity field of the slat and the slat shape integration can be written in a general form independent of the slat geometry parameters. The four slat geometry parameters are defined in the half-plane as illustrated in Fig. 4. These slat geometry parameters are the slat chord, c_2; the height of the slat midchord point above the real axis, f_1; the lateral offset of this midchord point from the imaginary axis, f_2; and the angle between the slat chord and the real axis, k_6.

The mapping from the half-plane W to the slat plane $S = s + it$ is a function of the slat geometry parameters only

$$S = (4/c_2)e^{+ik_6}[W - (f_2 + if_1)] \qquad (3)$$

This mapping translates the slat midchord to the S plane origin, rotates the entire plane by k_6 to place the slat chord along the $R(S)$ axis, and uniformly dilates figures in the half plane by the factor $4/c_2$.

The complex potential for the main flow in the slat plane is obtained by substituting the inverse of the slat plane mapping given by Eq. (3) into Eq. (2) which is the expression for the main flow complex potential $F(W)$ in the half-plane. The resulting expression for the complex potential $F(S)$ is then differentiated to obtain the complex conjugate velocity $\bar{q}(S) = dF(S)/dS$. Along the slat chord line, $(-2 \leqq s \leqq +2, t = 0)$, the parallel and normal components of the main flow velocity vector are given by the real and imaginary parts of $q(S)$, respectively.

Slat Representation as Distributed Singularities

In order to insure connectivity of the slat, a superposition of distributed singularities on the chord line is used to represent the slat. These distributed singularities correspond to the classical camber and thickness modes of thin airfoil theory written in complex variable form. The seven lowest order complex velocity functions are employed in this solution.[5,8] When superimposed, these five regular and two singular modes are sufficient to generate a representative range of slat camber and thickness distributions. Higher-order complex velocity functions are excluded because the induced velocity fields of the higher-order modes attenuate rapidly with distance from the slat chord line and thus are ineffective in modulating the main airfoil nose flow. Furthermore, higher-order modes can generate undesirable oscillations in the pressure distribution along the slat chord. However, alternate low-order complex velocity functions including thickness modes with nonzero trailing-edge angles can be selected from the extensive list given in Ref. 8 and can be readily incorporated into this solution.

Along the slat chord line, these seven complex velocity functions reduce to the Fourier modes of thin airfoil theory. If the chord station is defined in terms of the argument Θ as $s = 2\cos(\Theta)$, then the regular complex velocity functions have the classical $\sin(n\Theta)$ and $\cos(n\Theta)$ dependence, and the singular terms have the characteristic $\tan(\Theta/2)$ dependence. The four camber modes are designated as: the singular or flat plate camber mode, B_1; the first-order, parabolic arc camber mode, B_2; the second-order, reflexed camber mode, B_3; and the third-order, doubly inflected camber mode, B_4. Without altering the total slat circulation $\Gamma_s = 2\pi(B_1 + B_2)$, the regular B_3 and B_4 camber modes redistribute vorticity along the slat chord line. The three thickness modes are designated as: the primary or Joukowski thickness mode, which generates a nonzero slat leading edge radius; the second-order, lenticular thickness mode, B_6; and the third-order thickness mode, B_7, which has negative thickness behind the midchord point.

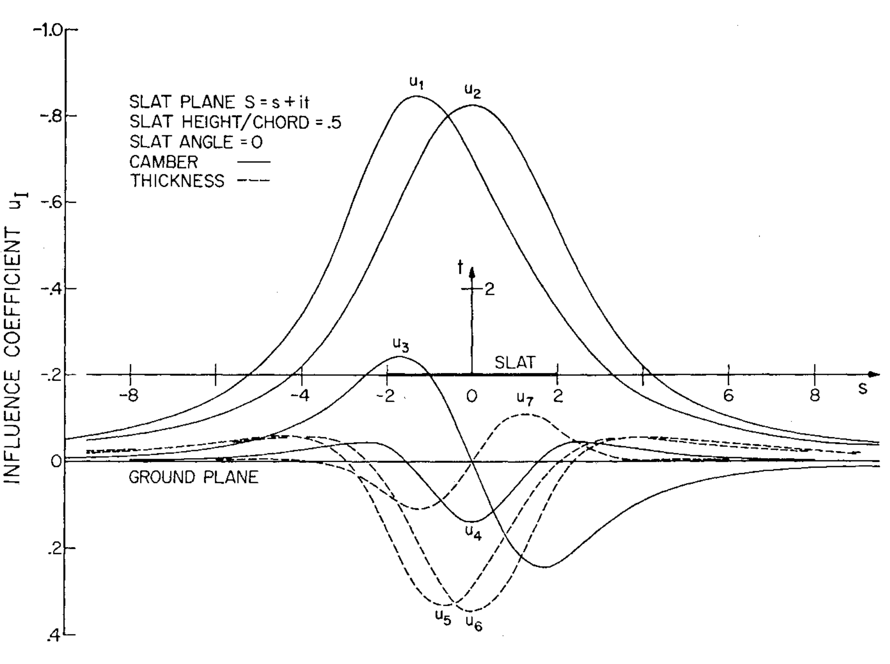

Fig. 5 Influence coefficients.

Both of the regular thickness modes, B_6 and B_7, are cusped at the leading and trailing edges.

Along the transformed ellipse nose surface which is designated the ground plane, the contribution to the total induced velocity field due to each of the distributed singularity modes on the slat can be readily evaluated. The slat plane flow is symmetric about the ground plane. Therefore, the induced velocity field of the image slat doubles the slat-induced parallel flow component along the ground plane and cancels the normal component of the slat field. Thus the total slat-induced velocity is twice the sum of the scalar products of the unit vector parallel to the ground plane and the seven complex velocity vectors corresponding to the slat singularity distribution modes.

The contributions to the induced velocity field by the seven slat modes are expressed in terms of influence coefficients. The influence coefficient u_{iI} is defined as the velocity component parallel to the ground plane which would be induced at the ith matching station on the ground plane by the Ith slat singularity distribution mode for a mode coefficient B_I equal to unity. These influence coefficients u_{iI} for the seven singularity distribution modes are the basic input for the linear least squares solution which is used to select the mode coefficients B_I required to match the specified modulating velocity field. Typical influence coefficients for a slat of zero inclination at a height-to-chord ratio of one-half are shown in Fig. 5.

Semi-Inverse Slat Design Technique

The initial step in this semi-inverse slat design technique is the determination of the modulating velocity distribution which the slat must induce in order to match the desired pressure distribution on the main airfoil. For the test cases, the desired pressure distribution was specified directly on an elliptical airfoil. The desired pressure coefficient is specified at an arbitrarily large number of matching stations in the critical high velocity region on the upper nose surface of the elliptical airfoil. The mapping derivatives of the transformation from the ellipse plane to the half-plane are then used to determine the corresponding specified velocity w_{i4} at each matching station on the $R(W)$ axis in the half-plane. The specified modulating velocity at each of the matching stations is defined as the difference between this specified velocity and the main flow velocity.

Selection of the slat location in the half-plane is the next major step of the semi-inverse solution. A fundamental characteristic of this slat design technique is that the fine modulation of the slat-induced velocity field is accomplished by adjusting the singularity distribution on the fixed slat chord line rather than by altering the position of a slat of fixed camber and thickness. An approximate specification of the slat location is therefore adequate, because the least squares solution for the singularity distribution mode coefficients B_I performs the fine matching to the specified modulating velocity distribution. For a set of slat locations within a local region of the half-plane, this semi-inverse solution will generate a class of slats of varying shape, all of which have induced velocity fields that closely match the desired induced field.

The insight required for the selection of an appropriate slat location and chord length is obtained by comparing a plot of the distribution of the specified modulating velocity along the $R(W)$ axis with the characteristic influence coefficient curves shown in Fig. 5. For typical small slat inclinations, the peak induced velocities for the singular B_1 and reflexed B_3 camber modes occur under the slat quarter chord, and the flow induced by the regular B_2 camber mode reaches a maximum under the slat midchord. Therefore, the slat offset from the origin, f_2, is selected to place the peak of the specified modulating velocity curve between the slat mid- and quarter-chord points. The appropriate slat chord and height f_1 are estimated from the width, the height-to-width ratio, and the tailoff slope of the specified modulating velocity curve. The slat angle k_6 is fixed by prescribing that the slat midchord be parallel to the main flow. Once the position of the slat chord line in the half-plane has been selected in this manner, the slat-induced modulating velocity can be expressed linearly in terms of the seven mode coefficients B_I and the influence coefficients u_{iI}.

As is apparent from the graphs of the influence coefficients (Fig. 5), positive values of the primary and first regular thickness mode coefficients, B_5 and B_6, induce positive velocities on the half-plane surface under the slat. Slat thickness thus increases the velocity past the ellipse nose. Because the purpose of the slat is to decrease the nose velocity by contributing a strong negative flow component, this detrimental effect of slat thickness must be counteracted by increased backflow induced by additional positive camber on the slat. From the design standpoint, therefore, slat thickness should be reduced as far as the requirements for adequate slat structural strength and an acceptable pressure distribution on the slat itself will permit.

In order to accommodate these practical constraints upon slat thickness, a minimum acceptable slat thickness distribution is specified as a superposition of the three thickness modes. The offset velocity w_{i5} corresponding to this prescribed slat thickness distribution can then be calculated at each matching station. A linear least squares solution is then conducted to select the four camber coefficients required to cancel this thickness-induced velocity field and match the specified modulating velocity distribution.

Linear Least-Squares Solution for Slat Mode Coefficients

For a particular slat geometry (slat chord, height, offset, and angle fixed), the total slat-induced velocity field w_{i1} at each of the matching stations is a linear function of the mode coefficients B_I. Although the regular velocity functions are orthogonal on the slat chord, their induced velocity fields on the inclined ground plane below the slat are not. A linear least squares technique[9] is, therefore, used to select the set of four camber mode coefficients which minimizes the sum of the squares of the differences between the biased specified modulating velocity and the slat-induced velocity at the matching stations. The biased specified modulating velocity w'_{i2} is defined as the difference between the specified velocity w_{i4} and the sum of the main flow velocity w_{i3} and the offset velocity w_{i5} induced by the prescribed slat thickness distribution.

$$w'_{i2} = w_{i4} - (w_{i3} + w_{i5}) \tag{4}$$

This least-squares technique solves the system of Eq. (5) for an

$$w'_{i2} = (8/c_2)(B_1 u_{i1} + B_2 u_{i2} + \cdots + B_4 u_{i4}) \tag{5}$$

arbitrarily large number of matching stations along the airfoil nose. The solution requires the inversion of a small (4 × 4) matrix which can be rapidly accomplished by a standard digital computer subroutine.

Determination of the Slat Shape

A lengthy nonlinear solution for the exact slat shape which corresponds to the singularity distribution determined by the least squares solution would be inconsistent with other inherent approximations in this semi-inverse design technique. A linearized integration is, therefore, used to determine the slat ordinates in the slat plane. The distortion of the slat due to the mild curvature of the main flowfield and the velocity field induced by the image slat are approximately taken into account.

In the slat plane, both the curvature and the convergence of the main flow streamlines are slight within the domain for efficient slats which is to the right of the origin near the real axis. For the elliptical airfoil test case, the main flow streamline pattern in the half-plane is shown in Fig. 3. If a straight slat chord line is placed approximately parallel to one of these main flow streamlines, the streamline curvature will affect the slat loading much more strongly than the streamline convergence will. Therefore, if the slat midchord is aligned with the local main flow in the half-plane, then the parallel component of the main flow can be assumed constant along the slat chord. Typically, the variation in the main flow parallel component is on the order of ten percent of the value at the slat midchord, and can be neglected. However, the velocity component normal to the slat chord line which exists due to the slight curvature of the main flow streamlines in the slat plane must be taken into account in the slat shape integration. Characteristically, the maximum value of this normal component of the main flow velocity vector is of the same order as the slat's self-induced normal velocity component along the chord line.

The velocity field induced on the slat by the distributed singularities on the image slat must also be taken into account in the determination of the slat shape. If the slat in the half-plane is considered as an airfoil in ground effect, a typical slat at a height-to-chord ratio of one half is well within the ground effect range in which the field of the image slat one chord away has significant influence. The solution for the image-induced velocity field on the slat is the same as a solution for the slat-induced velocity field on the ground plane if the slat geometry parameters are appropriately redefined. The same influence coefficient expressions can, therefore, be used to calculate both the velocity field induced by the slat on the ground plane and the field induced by the image slat on the slat. Applying the same approximations used for the main flow velocity components, the normal velocity component induced by the image slat is evaluated at each point on the slat chord line, but the parallel velocity component is approximated by the midchord value.

At each station along the slat chord line, the linearized tangential flow boundary condition is used to define the local slope of the slat surface. These local slopes are then integrated starting at the trailing edge of the slat chord line to obtain the slat ordinates. The normal velocity at each chord station is the sum of the contributions by the main flowfield, by the image slat field, and by the field induced by the singularity distributions on the slat itself. In accordance with the approximations described previously, the parallel velocity component is considered to be constant and equal to the sum of the main flow and image slat field contributions. The expressions for the normal velocity components can be readily integrated numerically using a standard integration subroutine. Alternatively, the integrals of the normal velocity components can be obtained analytically in terms of the slat geometry parameters and mode coefficients. The slat ordinates generated by this integration in the slat plane are then transformed point-by-point back to the ellipse plane.

The approximate velocity distribution on the slat can be readily obtained by Allen's technique.[10] To replace the two terms which are singular at the slat leading edge, the flow solution for the uncambered Joukowski airfoil corresponding to the B_5 primary thickness mode at the angle of attack appropriate to the flat plate camber mode B_1 is used. Because the other five modes are all regular at the slat leading edge, the parallel components of their induced velocity fields can be included as perturbations to this combined solution for the B_1 and B_5 modes. To a first order of approximation, the incorporation of the normal component of the main flowfield into the linearized slat shape integration distorts the slat to conform to the local curvature of the main flow streamlines and thereby removes the influence of the onset flow curvature on the slat loading.

First-Order Corrections to Slat Inclination and Ellipse Circulation

The singular or flat plate camber mode B_1 and the reflex camber mode B_3 can both contribute to a net angular offset between the geometrical mean line of the slat generated by the linearized integration and the assumed position of the slat singularity distribution along the real axis in the slat plate. A first-order correction for this angular offset can be readily incorporated in the solution. An initial least squares solution is conducted with the slat midchord aligned parallel to the main flow as described previously. Using the mode coefficients B_1 and B_3 from this initial solution, the two contributions to the net angular offset of the slat can be calculated. The slat angle is then redefined as the original slat inclination plus the two offsets. A second least squares solution is then conducted using the redefined slat angle. After this first-order correction to the slat inclination, the residual offset between the slat mean line and the slat plane real axis is small with respect to the slat height above the ground plane.

Because a small increment of compensating vorticity Γ_c is required to maintain the Kutta condition on the ellipse when a slat is added, an iteration on the least squares solution is conducted in order to improve the accuracy of the matching of the specified velocity distribution on the ellipse. When a leading-edge slat of circulation Γ_s is added near the nose of the ellipse, the vorticity of the image slat $\Gamma_i = -\Gamma_s$ is subtracted from the circulation of the ellipse. Because the image slat's negative vorticity is closer to the ellipse trailing edge than the vorticity on the slat itself, a small backflow or upward net velocity is induced at the trailing edge. An increment of compensating vorticity Γ_c at the ellipse center is, therefore, required to restore the Kutta condition by cancelling this backflow. In the far field, the vorticity distributions on the slat can be represented by two point vortices corresponding to the B_1 and B_2 vorticity distribution modes. The compensating vorticity required for each of these two substitution vortices can be readily determined in the circle plane. For realistically thin ellipses and efficient slats of small standoff from the nose, the compensating vorticity Γ_c ranges from approximately 3% to 0.5% of the basic ellipse circulation Γ_0.

An initial least squares solution is conducted with the total ellipse circulation Γ_t set equal to the basic circulation Γ_0 required to null the crossflow at the trailing edge of an unslatted ellipse. The camber mode coefficients from this initial solution are used to compute the compensating vorticity Γ_c required for the slat. A revised distribution of specified modulating velocity is then obtained by using revised values for the main flow velocity corresponding to the increased total ellipse circulation, $\Gamma_t = \Gamma_0 + \Gamma_c$. An additional least squares solution is then conducted to obtain the corrected camber mode coefficients. Typically, a complete semi-inverse solution required approximately 20 sec of computer time on an IBM System 360 Model 75.

Test Case Results

Comparison of Specified and Slat-Induced Modulations

For the test case, the desired pressure distribution was specified on an elliptical airfoil. The ellipse thickness ratio and angle of attack were selected to provide a realistic model of the flow environment in which a slat for a thin airfoil must operate. An ellipse with a nose radius of one percent of chord, a typical R_0 for a high-speed airfoil, was chosen. A lift coefficient of 2.12 which corresponds to an angle of attack of 17.2° was selected as representative for this 14.1% thick ellipse. As is shown in Fig. 6, without a leading-edge slat this ellipse would theoretically develop a severe leading-edge suction peak with a nose pressure coefficient equal to -21.8. The specified pressure distribution for the test case is also

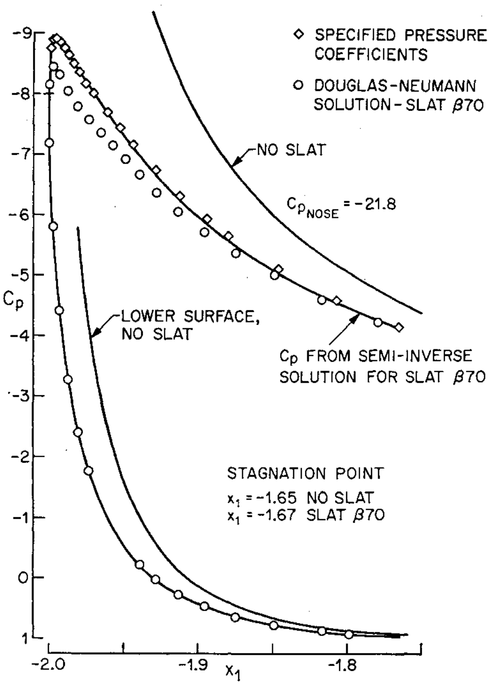

Fig. 6 Pressure distribution on ellipse nose.

shown in Fig. 6. This specified pressure distribution incorporates the general characteristics of a desirable nose pressure distribution, but is not intended to represent a separation-free pressure distribution for a particular full-scale airfoil.

The leading-edge slat generated by the semi-inverse solution for this test case was designated β70. A representative minimum acceptable thickness distribution corresponding to a slat thickness-to-chord ratio of 10% was specified, and the matrix inversion solution for the camber mode coefficients was then conducted. The pressure distribution calculated by this solution for the nose of the ellipse with slat β70 is also shown in Fig. 6. The very close agreement between the specified pressure distribution and the distribution achieved with this slat is typical of the accurate matching which can be accomplished with this semi-inverse design technique once an appropriate slat chord location in the half-plane has been selected. The effect of slat thickness on the slat-induced velocity field is illustrated in Fig. 7. The distributions of the specified modulating velocity w_{i2} and the biased specified modulating velocity w'_{i2} in the half-plane are both shown in this figure. The difference between the w_{i2} and w'_{i2} values is the offset velocity w_{i5} induced by the prescribed thickness distribution on the slat. Even for this very thin slat, the adverse velocity field induced by the slat thickness is significant.

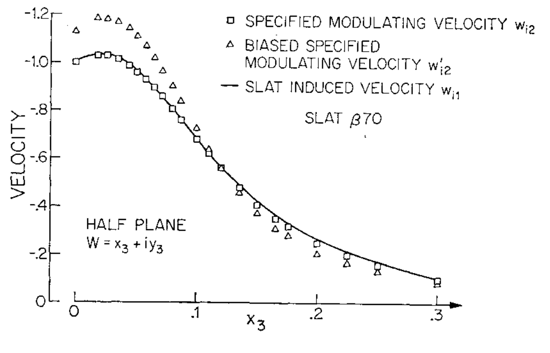

Fig. 7 Modulating velocity distributions.

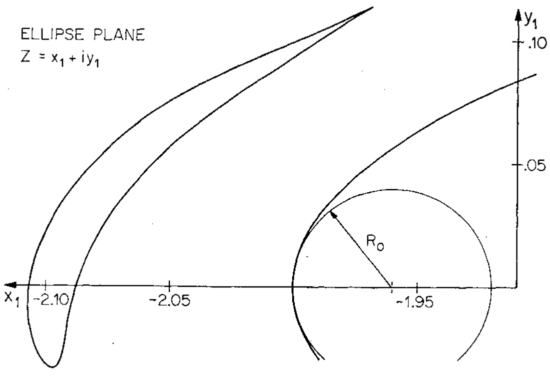

Fig. 8 Slat β70 configuration in ellipse plane.

For the test case slat β70, the corresponding slat shapes in the ellipse plane and in the slat plane are illustrated in Fig. 8 and Fig. 9, respectively. In the slat plane, the large reflex component of the slat camber distribution is evident. The effectiveness of the first-order correction to the slat inclination in reducing the offset between the slat's geometric mean line and the slat plane real axis to the same order as the slat thickness is also apparent in Fig. 9. The pressure distribution on the slat itself as calculated by the approximate technique incorporated in this semi-inverse solution is plotted in Fig. 10.

Comparison with Douglas-Neumann Direct Solution

For the slat β70 configuration, the flow solution calculated by this semi-inverse technique was compared with a direct potential flow solution computed by the Douglas-Neumann numerical technique.[6] On the ellipse nose, the direct and semi-inverse solutions are in close agreement. As is illustrated in Fig. 6, the maximum difference between the pressure coefficients predicted by the two solutions for the ellipse nose region is approximately four percent. On the slat itself, the pressure coefficients predicted by the direct solution and by

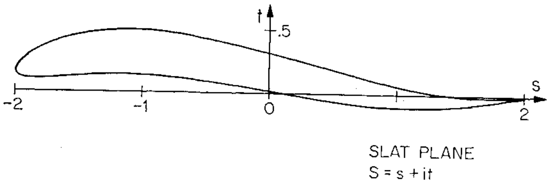

Fig. 9 Slat β70 in slat plane.

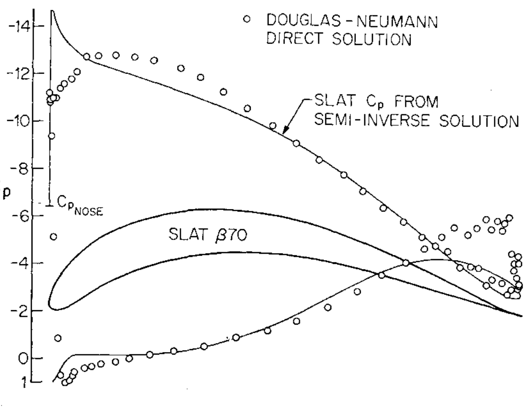

Fig. 10 Pressure distribution on slat β70.

this semi-inverse technique are in reasonable agreement over most of the slat chord but diverge at the slat leading and trailing edges as shown in Fig. 10. The scatter in the C_p values predicted by the direct solution near the trailing edge is an anomaly specific to this test case. The discrepancy between the present solution and the Douglas-Neumann at the slat leading edge is characteristic of linearized approximations near a leading edge. The accuracy of the present solution in the slat nose region could be improved by applying standard nonlinear corrections.

Comments

This paper does not deal with the problem of establishing the criteria for specifying desirable pressure distributions, a problem which involves boundary-layer analysis up to the point of separation. It is noted, however, that both the main airfoil and the slat must have acceptable pressure distributions. This semi-inverse technique enables a designer to place constraints upon the slat nose radius and thickness distribution to insure that severe adverse pressure gradients do not occur on the slat itself. It is also evident that there should be some off-design range of angle of attack over which the slat and airfoil operate without separation. Generally speaking, it may be assumed that this range need not be large because the slats are employed only in certain closely defined portions of the flight envelope.

It is of interest to observe that, although this paper is concerned only with incompressible flows, the reduction of adverse pressure gradients accomplished by a leading edge slat is accompanied by reductions in absolute velocities on the nose of the main airfoil. Thus the slat will generally have a favorable effect on compressible influences at high speeds. The criteria used for establishing desirable pressure distributions at high speeds will, of course, differ from those used for incompressible flows.

Once a slat configuration has been generated by this semi-inverse technique, pressure distributions at other angles of attack may be determined by using a standard direct solution such as the Douglas-Neumann numerical technique. These direct solutions require the inversion of a rather complex integral equation. Therefore, it is worthwhile to note that off-design solutions may be directly obtained from a single solution at a given angle of attack without solving any further integral equations by using the transformation of the slat and airfoil to a pair of flat plates. This mapping is implicitly contained in the single solution already determined. The process is outlined in Ref. 5.

Conclusions

The semi-inverse technique described in this paper provides a useful method for preliminary aerodynamic design of leading-edge slats. The technique will generate a slat which will induce the modulating field required to accurately match a specified pressure distribution on the nose of the main airfoil. The digital computer program used for the trial semi-inverse solutions for elliptical main airfoils is straight-forward and can be executed rapidly. Furthermore, this technique can be readily extended to generate slats for arbitrary airfoils. For a test slat geometry generated by this semi-inverse technique, the ellipse nose flow calculated by the Douglas-Neumann direct numerical solution agrees well with the flow predicted by the semi-inverse solution. The technique would be particularly valuable when combined with a computerized display of the slat generated so that the mechanical feasibility of the slat can be immediately assessed.

Several significant qualitative insights into the slat design problem are provided by the limited number of trial slats generated. For a thin airfoil with a severe suction peak at the nose, a small, thin, and highly cambered slat located close to the leading edge is desirable. For an efficient slat design, the slat vorticity should be concentrated near the region of the airfoil nose requiring the highest modulating backflow which is the first few percent of the airfoil chord. Furthermore, the slat standoff should be on the order of half of the slat chord or less so that the higher order slat camber modes can provide the precise modulation of the slat-induced velocity distribution required to accurately match the specified velocity distribution on the airfoil nose. At these low slat standoff-to-chord ratios, the adverse velocity field induced by the slat thickness distributions is of the same order as the desired backflow field induced by the slat camber distributions, and must be compensated for by additional slat vorticity. Therefore, the slat thickness should be reduced as far as the requirements for adequate slat structural strength and an acceptable pressure distribution on the slat itself will permit. Because the main flow streamlines near the nose of a heavily loaded airfoil are strongly curved, an efficient slat which will lie approximately along one of these streamlines must be very highly cambered.

References

[1] Lachmann, G. V., "Sir Frederick Handley-Page, The Man and His Work," *Journal of the Royal Aeronautical Society*, Vol. 68, No. 643, July 1964, pp. 433–452.

[2] Lindfield, A. W., "Brief Review of Theoretical Interpretations of the Slot Effect," *Boundary Layer and Flow Control*, edited by G. V. Lachmann, Vol. I, Pergamon Press, London, 1961.

[3] Cooke, J. C. and Brebner, G. C., "The Nature of Separation and its Prevention by Geometric Design in a Wholly Subsonic Flow," *Boundary Layer and Flow Control*, edited by G. V. Lachmann, Vol. 1, Pergamon Press, London, 1961.

[4] Schlicting, H., *Boundary Layer Theory*, 6th ed., McGraw-Hill, New York, 1968.

[5] O' Pray, J. E., "A Semi-Inverse Design Technique for Leading Edge Slats," thesis, June 1970, Dept. of Aeronautics, California Institute of Technology, Pasadena, Calif.

[6] Hess, J. L. and Smith, A. M. O., "Calculation of Potential Flow about Arbitrary Bodies," *Progress in Aeronautical Sciences*, Vol. 8, Pergamon Press, New York, 1966.

[7] Weber, J., "The Calculation of the Pressure Distribution Over the Surface of Two-Dimensional and Swept Wings with Symmetrical Aerofoil Sections," R&M 2918, 1956, Aeronautical Research Council, London.

[8] Jones, R. T. and Cohen, D., "Aerodynamics of Wings at High Speeds," *Aerodynamic Components of Aircraft at High Speeds*, Vol. 7, *High Speed Aerodynamics and Jet Propulsion*, edited by A. F. Donovan and H. R. Lawrence, Princeton University Press, Princeton, N.J., 1957, p. 15.

[9] Franklin, J. N., *Matrix Theory*, Prentice-Hall, Englewood Cliffs, N.J., 1968, p. 50.

[10] Allen, H. J., "General Theory of Airfoil Sections Having Arbitrary Shape or Pressure Distribution," Rept. 833, 1945, NACA.